Comput. Methods Appl. Mech. Engrg. 273 (2014) 238–254

Contents lists available at ScienceDirect

Comput. Methods Appl. Mech. Engrg.

journal homepage: www.elsevier.com/locate/cma

Gradient flows and variational principles for cardiac electrophysiology: Toward efficient and robust numerical simulations of the electrical activity of the heart

Daniel E. Hurtado [a,*], Duvan Henao [b]

[a] Department of Structural and Geotechnical Engineering and Biomedical Engineering Group, Pontificia Universidad Católica de Chile, Vicuña Mackenna 4860, Santiago, Chile
[b] Faculty of Mathematics, Pontificia Universidad Católica de Chile, Vicuña Mackenna 4860, Santiago, Chile

ARTICLE INFO

Article history:
Received 22 November 2013
Received in revised form 31 January 2014
Accepted 2 February 2014
Available online 8 February 2014

Keywords:
Cardiac electrophysiology
Variational principles
Gradient flow
FitzHugh–Nagumo
Saddle-point variational problems

ABSTRACT

The computer simulation of the electrical activity of the heart has experienced tremendous advances in the last decade. However, the acceptance of computational methods in the medical community will largely depend on their reliability, efficiency and robustness. In this work, we present a gradient-flow reformulation of the cardiac electrophysiology equations, and propose a minimax variational principle for the time-discretized electrophysiology problem. Based on results from variational analysis, we derive bounds on the time-step size that guarantee the existence and uniqueness of the saddle point, and in turn of the weak solution of the electrophysiology incremental problem. We also show conditions under which the minimax problem is equivalent to an effective minimization principle, which is amenable to a Rayleigh–Ritz finite-element analysis. The derived time-step bounds guarantee the strict convexity of the objective function resulting from spatial discretization, thus ensuring the convergence of gradient-descent methods. The proposed theory is applied to the widely employed FitzHugh–Nagumo model, which is shown to conform to the variational framework proposed in this work. The applicability of the method and its implications on the robustness of time integration are demonstrated by way of numerical simulations of the electrical behavior in a single-cell and 3D wedge and biventricular geometries. We envision that the proposed framework will open the door to the development of robust and efficient electrophysiology models and simulations.

1. Introduction

Computational cardiology has experienced important advances in the last decade with the advent of supercomputing platforms. The computer simulation of the propagation of electrical impulses in the cardiac muscle has received a great deal of attention from the computational science community [33]. Currently, detailed anatomical computational models of the electrophysiology of heart are being used to study the physiology and pathology of the heart [45]. The majority of these models are multiscale in spirit, and therefore prove very useful in understanding the behavior of cellular- and tissue-level mechanisms from the study of organ-level behavior [23]. The translation of such computational models into the clinic is currently being advocated by many research groups around the world [20]. However, the acceptance of computational methods in the

* Corresponding author. Tel.: +56 2 2354 4211.
E-mail address: dhurtado@ing.puc.cl (D.E. Hurtado).

http://dx.doi.org/10.1016/j.cma.2014.02.002
0045-7825/

medical community will largely depend on their efficiency, robustness and reliability, which are currently open avenues of research.

Cardiac electrophysiology concerns the study of the propagation and interaction of electrical waves in biological tissue. The roots of the mathematical formulation of electrophysiological models date back to the efforts of Hodgkin and Huxley [22] on modeling the electrical propagation in squid giant axons. Following the seminal work of Hodgkin and Huxley, a large number of cardiac electrophysiology models of the Purkinjee fibers, myocardial tissue and pacemaker cells have been proposed in the literature, see [14] for a comprehensive survey. Today, we distinguish two main classes of electrophysiological models: biophysical and phenomenological models [38]. Biophysical models [34,3,30,44] aim at describing the complex exchanges occurring at the sarcolemma, or cell membrane, and organelles by quantifying the sub-cellular fluxes of Calcium, Potassium, Sodium and Chlorides ions through the several different mechanisms available, i.e., ion channels, pumps, exchangers and gap junctions. Phenomenological models [16,32,1,15] aim at modeling a larger spatial and temporal scale than biophysical models, and they consider a reduced set of state variables and parameters that do not necessarily have a direct physical meaning but make these models more tractable from a mathematical analysis and computational implementation viewpoint.

Regardless of their nature, virtually all deterministic cardiac electrophysiology models fall in the category of non-linear reaction–diffusion equations [27]. The numerical solution of cardiac electrophysiology equations has been predominantly carried out using finite-difference [42,8,36], finite-volume [21,26] and finite-element [40,48] approximations for the spatial discretization, whereas the time integration has been predominantly addressed by finite-difference schemes. The most traditional time-integration schemes used in cardiac electrophysiology are explicit Euler methods, which have proven particularly suitable for large-scale simulations where solving a large linear system of equations is generally avoided. However, it is well known that time-step bounds that arise from stability considerations for explicit methods become more stringent as the mesh size decreases, thus reducing the efficiency of those methods as a finer spatial discretization is considered. Moreover, the determination of stability conditions can become cumbersome or even intractable when dealing with highly non-linear systems. In the search of more stable algorithms, semi-implicit and fully-implicit [29] schemes have also been employed, allowing for larger time steps at the expense of solving a nonlinear set of equations at each time step. Depending on the electrophysiology model, the resulting set of equations can be highly nonlinear, and even contain discontinuous functions. As a consequence, the convergence of classical solution methods can hardly be guaranteed, thus hindering the robustness of implicit methods.

The mathematical analysis of electrophysiology models has been mainly developed during the last decade, following the popularization of the numerical simulation of cardiac electrical activity by the scientific computing community. The proof of existence and uniqueness of solutions to the phenomenological FitzHugh–Nagumo bidomain model was developed by Colli Franzone and Savaré [6] based on classical results from the general theory of evolution variational inequalities. Using the same abstract variational framework, Sanfelici [41] has shown the convergence of Galerkin finite-element approximations of the FitzHugh–Nagumo model. More recently, a multiscale analysis based on the Γ-convergence theory has shown the adequacy of the bidomain model to represent the microscopic behavior of cardiac tissue [37]. Recent advances showing the existence and uniqueness of solutions to more complex biophysical models have been addressed in [47].

Although it was observed in [6] that the FitzHugh–Nagumo equations have a variational structure, this fundamental property and its implications have not been exploited to date, neither by the biophysical nor the computational communities. In this work, we present a gradient-flow reformulation of the cardiac electrophysiology equations that allows one to understand these models in a new light, namely, in terms of variational principles such as minimization of free energy, maximization of entropy, and phase transitions, which are pervasive in the thermodynamics, mechanics, electromagnetism, and the biophysics literature. From a mathematical viewpoint, variational principles offer a wealth of analysis results regarding existence of solutions using the tools of the modern calculus of variations [9]. From a numerical point of view, variational principles are the underlying framework for some of the most celebrated numerical methods, like the finite element method [7]. Variational formulations for gradient-flow systems have been applied to a wide variety of physics and engineering problems, particularly by the computational mechanics community in the formulation and numerical solution of multiscale material models [35,24,25] and soft-tissue biomechanics [49,12].

The paper is organized as follows. Section 2 is concerned with the theoretical aspects of the variational principle for cardiac electrophysiology introduced in this work. We start by stating, in a general form, the initial boundary value problem that governs the electrical behavior of cardiac tissue. Generalized potentials are then introduced, and a gradient-flow reformulation of the electrophysiology problem based on such potentials is presented. Using a Backward-Euler time-discretization scheme, an incremental minimax variational formulation equivalent to the time-discretized governing equations is introduced, and conditions on the time-step size are stated in order to guarantee existence and uniqueness of saddle points. Exploiting the local nature of the evolution equations for the state variables, an effective minimization problem amenable to non-linear finite-element methods is derived. The phenomenological FitzHugh–Nagumo model is then analyzed in view of the proposed theory, and bounds on the time-step size that only depend on the parameters of the model are derived to ensure strict convexity of the effective minimization problem. The time-step bound, in turn, guarantees existence and uniqueness of the weak solution. In Section 3, we employ the proposed method to numerically solve three examples of increasing geometrical complexity. The convergence of the solution to the non-linear problem for each example is studied and analyzed based on the time-step bounds derived for the FitzHugh–Nagumo model. Section 4 ends with a discussion on the obtained results and future perspectives.

2. Variational principle for the electrophysiology problem

Let $\mathcal{B} \subset \mathbb{R}^N$ be the physical domain of interest where N is any positive integer, $\phi : \mathcal{B} \times \mathbb{R}^+ \to \mathbb{R}$ the scaled transmembrane potential, and $\boldsymbol{r} = (r_1, \ldots, r_M) : \mathcal{B} \times \mathbb{R}^+ \to \mathbb{R}^M$ the internal-variable vector that controls the recovery of the cell. The general electrophysiology problem can be written in terms of the nonlinear reaction–diffusion system of equations

$$C_\phi \dot{\phi} + \operatorname{div} \boldsymbol{q} = f^\phi(\phi, \boldsymbol{r}), \tag{1}$$

$$\boldsymbol{C}_r \dot{\boldsymbol{r}} = \boldsymbol{f}^{\,r}(\phi, \boldsymbol{r}), \tag{2}$$

where $\dot{(\square)} = \frac{\partial \square}{\partial t}$ denotes time differentiation, $C_\phi \in \mathbb{R}_+$, and $\boldsymbol{C}_r \in \mathbb{R}^{M \times M}$ is symmetric and positive definite tensor. Here we have considered the simplified mono-domain formulation which depends only on the transmembrane potential and internal variables, instead of the bi-domain formulation, where both intracellular and extracellular potentials need to be described independently. The flux term $\boldsymbol{q}$ characterizes the propagating nature of excitation waves, which we assume to take the form (Fick's law)

$$\boldsymbol{q} = -\boldsymbol{D} \nabla \phi. \tag{3}$$

where $\boldsymbol{D} \in \mathbb{R}^{N \times N}_+$ is a symmetric and positive-definite conductivity tensor. Dirichlet and Neumann boundary conditions complement the governing equations,

$$\phi = \bar{\phi}, \quad \boldsymbol{x} \in \partial \mathcal{B}_\phi, \tag{4}$$

$$\boldsymbol{q} \cdot \boldsymbol{n} = \bar{q}, \quad \boldsymbol{x} \in \partial \mathcal{B}_q. \tag{5}$$

Initial conditions read

$$\phi|_{t=0} = \phi_0(\boldsymbol{x}), \tag{6}$$

$$\boldsymbol{r}|_{t=0} = \boldsymbol{r}_0(\boldsymbol{x}). \tag{7}$$

The choice of the recovery variable $\boldsymbol{r}$ and source terms f^ϕ and $\boldsymbol{f}^{\,r} = (f^r_1, \ldots f^r_M)$ determines the particular electrophysiology formulation, and there are a plethora of different formulations in the literature. For an extensive review of the most popular electrophysiology models, the reader is referred to [14]. The existence and uniqueness of the mono-domain electrophysiology problem has been addressed by ColliFranzone and Savaré [6].

We now consider the time integration of the electrophysiology Eqs. (1) and (2). Consider the generic time interval $[t_n, t_{n+1}]$, $n \in \mathbb{Z}$ where all the information at $t = t_n$ is assumed to be known. Using a Backward-Euler finite-difference scheme in time, the semi-discrete electrophysiology equations read

$$C_\phi \frac{\phi_{n+1} - \phi_n}{\Delta t} - \operatorname{div}(\boldsymbol{D} \nabla \phi_{n+1}) = f^\phi(\phi_{n+1}, \boldsymbol{r}_{n+1}) \tag{8}$$

$$\boldsymbol{C}_r \frac{\boldsymbol{r}_{n+1} - \boldsymbol{r}_n}{\Delta t} = \boldsymbol{f}^{\,r}(\phi_{n+1}, \boldsymbol{r}_{n+1}), \tag{9}$$

where $\Delta t = t_{n+1} - t_n$. This time discretization scheme has been widely employed in the numerical solution of electrophysiology equations [19,50,23] due to stability considerations, at the expense of solving a nonlinear problem for each time step.

2.1. Generalized potentials and gradient-flow reformulation

In the sequel, we seek to reformulate the electrophysiology problem into a gradient-flow system. Let $\mathcal{E}$ be the generalized electrochemical potential, and Ψ the rate potential. A system has a gradient-flow structure if the governing equations are recovered from

$$0 \in \partial \Psi + D\mathcal{E}, \tag{10}$$

where D is the Fréchet derivative and ∂ signifies the subdifferential operator. The reader is referred to [2] to see more about the application of subdifferentials in reaction–diffussion and gradient-flow problems. In (10), $D\mathcal{E}$ represents a driving force that controls the evolution of the system. For the case of the general electrophysiology model, we define the generalized electrochemical potential as

$$\mathcal{E}[\phi, \boldsymbol{r}] := \int_{\mathcal{B}} E(\phi, \nabla \phi, r)\, \mathrm{d}\boldsymbol{x} + \int_{\mathcal{B}_q} \phi \bar{q}\, \mathrm{d}S = \int_{\mathcal{B}} \left\{ \frac{1}{2} \nabla \phi \cdot \boldsymbol{D} \nabla \phi + F(\phi, \boldsymbol{r}) \right\} \mathrm{d}\boldsymbol{x} + \int_{\partial \mathcal{B}_q} \phi \bar{q}\, \mathrm{d}S, \tag{11}$$

where $E : \mathbb{R} \times \mathbb{R}^N \times \mathbb{R} \to \mathbb{R}$ is the electrochemical potential density, and $F : \mathbb{R} \times \mathbb{R}^M \to \mathbb{R}$ is a function such that

$$\frac{\partial F}{\partial \phi} = -f^\phi(\phi, \boldsymbol{r}) \tag{12}$$

$$\frac{\partial F}{\partial r_i} = f^r_i(\phi, \boldsymbol{r}), \quad i = 1, \ldots, M. \tag{13}$$

We also define the rate potential as

$$\Psi[\dot{\phi},\dot{\boldsymbol{r}}] := \int_{\mathcal{B}} \psi(\dot{\phi},\dot{\boldsymbol{r}})\,\mathrm{d}\boldsymbol{x}, = \int_{\mathcal{B}} \left\{\frac{1}{2}C_\phi\dot{\phi}^2 - \frac{1}{2}\dot{\boldsymbol{r}}\cdot\boldsymbol{C}_r\dot{\boldsymbol{r}}^2\right\}\mathrm{d}\boldsymbol{x}. \tag{14}$$

It follows that Eqs. (1) and (2) can be recovered from the potentials just defined, thus conferring the general electrophysiology model a gradient-flow structure. We remark that while the rate potential is a strictly convex functional in $\dot{\phi}$, the electrochemical potential need not be convex in ϕ.

2.2. Time discretization: incremental variational formulation

In the following, we draw ideas from the solid mechanics community [17,35] and develop an incremental variational formulation by partitioning the temporal space into a sequence of finite intervals. Before stating our result we introduce some assumptions and notation. The *incremental potential density* is defined as

$$g_n(\phi,\nabla\phi,\boldsymbol{r}) := \Delta t\,\psi\left(\frac{\phi-\phi_n}{\Delta t},\frac{\boldsymbol{r}-\boldsymbol{r}_n}{\Delta t}\right) + E(\phi,\nabla\phi,\boldsymbol{r}), \tag{15}$$

where $\Delta t = t_{n+1} - t_n$, and the corresponding incremental potential is defined as

$$G_n[\phi,\boldsymbol{r}] := \int_{\mathcal{B}} g_n(\phi,\nabla\phi,\boldsymbol{r})\,\mathrm{d}\boldsymbol{x} - \int_{\partial\mathcal{B}_q}\phi\bar{q}\,\mathrm{d}S. \tag{16}$$

It will be assumed henceforth that the potential $F(\phi,\boldsymbol{r})$ in (11) is of class $C^2(\mathbb{R}\times\mathbb{R}^M,\mathbb{R})$ and there exist exponents $\gamma,q>1$ such that

$$|F(\phi,\boldsymbol{r})| \leqslant A(|\phi|^q + |\boldsymbol{r}|^\gamma) + B, \tag{17}$$

$$|f^\phi(\phi,\boldsymbol{r})| \leqslant A\left(|\phi|^{q-1} + |\boldsymbol{r}|^{\frac{\gamma(N+2)}{2N}}\right) + B, \quad \text{and} \tag{18}$$

$$|\boldsymbol{f}^{\,r}(\phi,\boldsymbol{r})| \leqslant A\left(|\phi|^{q\left(1-\frac{1}{\gamma}\right)} + |\boldsymbol{r}|^{\gamma-1}\right) + B, \tag{19}$$

for all $(\phi,\boldsymbol{r})\in\mathbb{R}\times\mathbb{R}^M$ and some constants $A,B>0$. Further, in the case where $N\geqslant 3$ we assume that $q\leqslant 2^* := \frac{2N}{N-2}$. The transmembrane potential ϕ and state variable $\boldsymbol{r}$ will be assumed to belong to the functional spaces

$$\mathcal{S} = \left\{\phi\in H^1(\mathcal{B}) : \phi = \bar{\phi} \text{ in } \partial\mathcal{B}_\phi\right\} \quad \text{and} \quad \mathcal{V} = L^\gamma(\mathcal{B},\mathbb{R}^M), \tag{20}$$

respectively, where $\gamma>1$ is the exponent in (17). The smallest eigenvalues of $\boldsymbol{C}_r$ and $\boldsymbol{D}$ will be denoted by $C_r^{\min}$ and μ, respectively. The ellipticity constants δ_ϕ and δ_r are defined by

$$\delta_\phi := \sup_{(\phi,\boldsymbol{r})\in\mathbb{R}\times\mathbb{R}^M} \frac{\partial f^\phi}{\partial\phi}(\phi,\boldsymbol{r}) \quad \text{and} \quad \delta_r := \sup_{\substack{(\phi,\boldsymbol{r})\in\mathbb{R}\times\mathbb{R}^M,\\ \xi\in\mathbb{R}^M,|\xi|\leqslant 1}} \xi\cdot(\nabla_{\boldsymbol{r}}\boldsymbol{f}^{\,r}(\phi,\boldsymbol{r}))\xi. \tag{21}$$

Finally, $C_{\mathcal{B}} = C_{\mathcal{B}}(\mathcal{B},\partial\mathcal{B}_\phi)$ denotes the optimal constant in the Poincaré inequality

$$\int_{\mathcal{B}}\eta(\boldsymbol{x})^2\,\mathrm{d}\boldsymbol{x} \leqslant C_{\mathcal{B}}\int_{\mathcal{B}}|\nabla\eta(\boldsymbol{x})|^2\,\mathrm{d}\boldsymbol{x} \quad \forall\ \eta\in H^1(\mathcal{B}) \text{ s.t. } \eta = 0 \text{ on } \partial\mathcal{B}_\phi. \tag{22}$$

Theorem 1. *Let $F, G_n, \mathcal{S}, \mathcal{V}, C_r^{\min}, \mu, \delta_\phi, \delta_r$ and $C_{\mathcal{B}}$ be as above. Suppose, further, that*

$$\frac{1}{\Delta t} > \max\left\{\frac{\delta_\phi}{C_\phi} - \frac{\mu}{C_\phi C_{\mathcal{B}}}, \frac{\delta_r}{C_r^{\min}}\right\} \tag{23}$$

and that $\bar{q}\in L^2(\partial\mathcal{B}_q)$. Then, the weak form of the semi-discrete electrophysiology equations (4), (5), (8) and (9), given by

$$\int_{\mathcal{B}}\left\{C_\phi\frac{\phi_{n+1}-\phi_n}{\Delta t}\eta + \boldsymbol{D}\nabla\phi\cdot\nabla\eta - f^\phi(\phi,\boldsymbol{r})\eta\right\}\mathrm{d}\boldsymbol{x} - \int_{\partial\mathcal{B}_q}\bar{q}\eta\,\mathrm{d}S = 0, \quad \forall\ \eta\in H_0^1(\mathcal{B}) \tag{24}$$

$$\int_{\mathcal{B}}\left\{\boldsymbol{C}_r\frac{\boldsymbol{r}_{n+1}-\boldsymbol{r}_n}{\Delta t} - \boldsymbol{f}^{\,r}(\phi_{n+1},\boldsymbol{r}_{n+1})\right\}\boldsymbol{\xi}\,\mathrm{d}\boldsymbol{x} = 0, \quad \forall\ \boldsymbol{\xi}\in L^\gamma(\mathcal{B},\mathbb{R}^M), \tag{25}$$

admits a unique solution $(\phi_{n+1},\boldsymbol{r}_{n+1})$ determined by the variational principle

$$G_n[\phi_{n+1},\boldsymbol{r}_{n+1}] = \min_{\phi\in\mathcal{S}}\max_{\boldsymbol{r}\in\mathcal{V}} G_n[\phi,\boldsymbol{r}]. \tag{M}$$

Remark 1. The theorem remains true, with the same proof, if $F(\phi,\boldsymbol{r})$ is only C^1 but such that

$$F(\phi,\boldsymbol{r}) - F(\phi_0,\boldsymbol{r}) \geqslant -f^\phi(\phi_0,\boldsymbol{r})(\phi-\phi_0) + \frac{\delta_\phi}{2}(\phi-\phi_0)^2 \quad \forall\ \phi,\phi_0\in\mathbb{R}, \quad \boldsymbol{r}\in\mathbb{R}^M \tag{26}$$

$$\text{and} \quad F(\phi,\boldsymbol{r}) - F(\phi,\boldsymbol{r}_0) \leqslant \boldsymbol{f}^{\,r}(\phi,\boldsymbol{r}_0)\cdot(\boldsymbol{r}-\boldsymbol{r}_0) + \frac{\delta_r}{2}|\boldsymbol{r}-\boldsymbol{r}_0|^2 \quad \forall\ \phi\in\mathbb{R}, \quad \boldsymbol{r},\boldsymbol{r}_0\in\mathbb{R}^M \tag{27}$$

for some constants $\delta_\phi,\delta_r\in\mathbb{R}$.

Remark 2. The reason for stating (23) as a condition on $\frac{1}{\Delta t}$ (and not directly on Δt) is that the expression on the right can be negative. If $F(\phi, \boldsymbol{r})$ is convex in ϕ, the condition on the time step reads $\delta_r \Delta t < C_r^{\min}$. If $F(\phi, \boldsymbol{r})$ is concave in $\boldsymbol{r}$, it reads $\frac{1}{\Delta t} > \frac{\delta_\phi}{C_\phi} - \frac{\mu}{C_\phi C_{\mathcal{B}}}$. If it is both convex in ϕ and concave in $\boldsymbol{r}$, the conclusion holds for every $\Delta t > 0$.

Theorem 1 follows from several results of convex analysis and minimax theory (see, e.g. [11, Chapter VI, Propositions 1.5, 1.6 and 2.2]), which we briefly recall.

Definition 1. Let $\mathcal{V}$ and $\mathcal{W}$ be vector spaces and let $G : \mathcal{S} \times \mathcal{V} \to \mathbb{R}$, where $\varnothing \neq \mathcal{S} \subset \mathcal{W}$ is convex.

(i) A pair $(\phi_0, \boldsymbol{r}_0) \in \mathcal{S} \times \mathcal{V}$ is a saddle point of G if

$$G[\phi_0, \boldsymbol{r}] \leqslant G[\phi_0, \boldsymbol{r}_0] \leqslant G[\phi, \boldsymbol{r}_0] \quad \forall\ (\phi, \boldsymbol{r}) \in \mathcal{S} \times \mathcal{V}.$$

(ii) The functional G is convex-concave if

$$G[(1-\lambda)\phi_1 + \lambda\phi_2, \boldsymbol{r}] \leqslant (1-\lambda)G[\phi_1, \boldsymbol{r}] + \lambda G[\phi_2, \boldsymbol{r}] \quad \forall\ \phi_1, \phi_2 \in \mathcal{S},\ \boldsymbol{r} \in \mathcal{V},\ \lambda \in [0,1]$$

and

$$G[\phi, (1-\lambda)\boldsymbol{r}_1 + \lambda\boldsymbol{r}_2] \geqslant (1-\lambda)G[\phi, \boldsymbol{r}_1] + \lambda G[\phi, \boldsymbol{r}_2] \quad \forall\ \phi \in \mathcal{S},\ \boldsymbol{r}_1, \boldsymbol{r}_2 \in \mathcal{V},\ \lambda \in [0,1].$$

If the above inequalities are strict for $\lambda \in (0,1)$ then G is strictly convex-concave.

(iii) The functional G is Gâteaux-differentiable at (ϕ_0, r_0) if $\mathcal{W}$ and $\mathcal{V}$ are normed spaces and the partial derivatives

$$\langle D_\phi G[\phi_0, \boldsymbol{r}_0], \phi - \phi_0 \rangle := \lim_{\lambda \to 0^+} \frac{G[\phi_\lambda, \boldsymbol{r}_0] - G[\phi_0, \boldsymbol{r}_0]}{\|\phi_\lambda - \phi_0\|}, \quad \phi_\lambda = \lambda\phi + (1-\lambda)\phi_0$$

$$\langle D_r G[\phi_0, \boldsymbol{r}_0], \boldsymbol{r} - \boldsymbol{r}_0 \rangle := \lim_{\lambda \to 0^+} \frac{G[\phi_0, \boldsymbol{r}_\lambda] - G[\phi_0, \boldsymbol{r}_0]}{\|\boldsymbol{r}_\lambda - \boldsymbol{r}_0\|}, \quad \boldsymbol{r}_\lambda = \lambda\boldsymbol{r} + (1-\lambda)\boldsymbol{r}_0$$

exist for all $(\phi, \boldsymbol{r}) \in \mathcal{S} \times \mathcal{V}$ and can be extended as linear functionals in $\mathcal{W}^*$ and $\mathcal{V}^*$.

Proposition 1. *Let $\mathcal{W}$ and $\mathcal{V}$ be reflexive Banach spaces. Suppose that $\varnothing \neq \mathcal{S} \subset \mathcal{W}$ is closed and convex and that $G : \mathcal{S} \times \mathcal{V} \to \mathbb{R}$ is a convex-concave functional. Also assume that*

(i) *for all $\phi \in \mathcal{S}, \boldsymbol{r} \mapsto G[\phi, \boldsymbol{r}]$ is upper semicontinuous and $\lim_{\boldsymbol{r} \in \mathcal{V}} G[\phi, \boldsymbol{r}] = -\infty$;*

(ii) *for all $\boldsymbol{r} \in \mathcal{V}, \phi \mapsto G[\phi, \boldsymbol{r}]$ is lower semicontinuous and $\lim_{\substack{\phi \in \mathcal{S} \\ \|\phi\| \to \infty}} G[\phi, \boldsymbol{r}] = +\infty$.*

Then G has at least one saddle point $(\phi_0, \boldsymbol{r}_0)$ and every saddle point is such that

$$G[\phi_0, \boldsymbol{r}_0] = \min_{\phi \in \mathcal{S}} \max_{\boldsymbol{r} \in \mathcal{V}} G[\phi, \boldsymbol{r}] = \max_{\boldsymbol{r} \in \mathcal{V}} \min_{\phi \in \mathcal{S}} G[\phi, \boldsymbol{r}].$$

If, moreover, G is Gâteaux-differentiable, then $(\phi_0, \boldsymbol{r}_0)$ is a saddle-point of G if and only it satisfies the weak form of the Euler–Lagrange equations

$$\langle D_\phi G, \phi - \phi_0 \rangle \geqslant 0, \quad \langle D_r G, \boldsymbol{r} - \boldsymbol{r}_0 \rangle \leqslant 0 \quad \forall \phi \in \mathcal{S}, \boldsymbol{r} \in \mathcal{V}.$$

If, further, G is strictly convex-concave, then the saddle point is unique.

Proof of Theorem 1. By the Sobolev embedding and the trace theorems (see, e.g. [13, Theorems 5.5.1 and 5.6.2]) and the assumption on the growth of $F(\phi, \boldsymbol{r})$, the map $G_n[\phi, \boldsymbol{r}]$ is well defined as a function from $\mathcal{S} \times \mathcal{V}$ to $\mathbb{R}$ (that is, the integrals in (16) are finite). Again by Sobolev's embedding theorem (combined with generalized dominated convergence), it follows that $G_n[\phi, \boldsymbol{r}]$ is continuous in ϕ and in $\boldsymbol{r}$ with respect to convergence in norm in $H^1(\mathcal{B})$ and $L^\gamma(\mathcal{B})$, respectively.

In order to apply Proposition 1, it is necessary to prove that if the hypothesis on the time step is satisfied then $G_n[\phi, \boldsymbol{r}]$ is strictly convex-concave. To this aim, fix first $\boldsymbol{r} \in \mathcal{V}$ and let $\phi_1, \phi_2 \in \mathcal{S}$ and $\lambda \in (0,1)$. A direct calculation shows that

$$\frac{2}{\lambda(1-\lambda)}\left(((1-\lambda)G_n[\phi_1, \boldsymbol{r}] + \lambda G_n[\phi_2, \boldsymbol{r}]) - G_n[(1-\lambda)\phi_1 + \lambda\phi_2, \boldsymbol{r}]\right) \tag{28}$$

$$= \int_{\mathcal{B}} \left\{ \frac{C_\phi}{h}(\phi_2 - \phi_1)^2 + \nabla(\phi_2 - \phi_1) \cdot \boldsymbol{D} \nabla(\phi_2 - \phi_1) + \left(\inf_{\mathbb{R} \times \mathbb{R}^M} \frac{\partial^2 F}{\partial \phi^2} \right) (\phi_2 - \phi_1)^2 \right\} \mathrm{d}\boldsymbol{x} \tag{29}$$

$$\geqslant \left(\frac{C_\phi}{h} - \delta_\phi \right) \int_{\mathcal{B}} (\phi_2 - \phi_1)^2 \,\mathrm{d}\boldsymbol{x} + \mu \int_{\mathcal{B}} |\nabla(\phi_2 - \phi_1)|^2 \,\mathrm{d}\boldsymbol{x} \tag{30}$$

$$\geqslant \left(\frac{C_\phi}{h} + \frac{\mu}{C_{\mathcal{B}}} - \delta_\phi \right) \int_{\mathcal{B}} (\phi_2 - \phi_1)^2 \,\mathrm{d}\boldsymbol{x}, \tag{31}$$

which implies that $G_n[\cdot,\boldsymbol{r}]$ is strictly convex for every $\boldsymbol{r}\in\mathcal{V}$. Analogously, $G_n[\phi,\boldsymbol{r}]$ is strictly concave in $\boldsymbol{r}$ since for every $\boldsymbol{r}_1,\boldsymbol{r}_2\in\mathcal{V}$, $\phi\in\mathcal{S}$, and $\lambda\in(0,1)$

$$\frac{2}{\lambda(1-\lambda)}(((1-\lambda)G_n[\phi,\boldsymbol{r}_1]+\lambda G_n[\phi,\boldsymbol{r}_2])-G_n[\phi,(1-\lambda)\boldsymbol{r}_1+\lambda\boldsymbol{r}_2]) \tag{32}$$

$$\leqslant\int_{\mathcal{B}}\left\{-\frac{(\boldsymbol{r}_2-\boldsymbol{r}_1)\cdot\boldsymbol{C}_r(\boldsymbol{r}_2-\boldsymbol{r}_1)}{h}+\delta_r|\boldsymbol{r}_2-\boldsymbol{r}_1|^2\right\}\mathrm{d}\boldsymbol{x}\leqslant\left(-\frac{C_r^{\min}}{h}+\delta_r\right)\int_{\mathcal{B}}|\boldsymbol{r}_2-\boldsymbol{r}_1|^2\,\mathrm{d}\boldsymbol{x}. \tag{33}$$

The proof that G_n is Gâteaux-differentiable whenever $F(\phi,\boldsymbol{r})$ satisfies the growth conditions (17)–(19), and that its partial derivatives are given by

$$\langle D_\phi G_n[\phi,\boldsymbol{r}],\eta\rangle=\int_{\mathcal{B}}\left\{C_\phi\frac{\phi-\phi_n}{h}\eta+\boldsymbol{D}\nabla\phi\cdot\nabla\eta-f^\phi(\phi,r)\eta\right\}\mathrm{d}\boldsymbol{x}-\int_{\partial\mathcal{B}_q}\bar{q}\eta\,\mathrm{d}S,\quad\forall\ \eta\in H_0^1(\mathcal{B})$$

$$\langle D_r G_n[\phi,\boldsymbol{r}],\boldsymbol{\xi}\rangle=\int_{\mathcal{B}}\left\{-\boldsymbol{C}_r\frac{\boldsymbol{r}_{n+1}-\boldsymbol{r}_n}{h}+f^r(\phi_{n+1},\boldsymbol{r}_{n+1})\right\}\boldsymbol{\xi}\,\mathrm{d}\boldsymbol{x},\quad\forall\ \boldsymbol{\xi}\in\mathcal{L}^\gamma(\mathcal{B},\mathbb{R}^M)$$

is standard and can be found, e.g. in [9, Theorem 3.11 and Example 3.4.1] (Even though is not explicitly stated, the same proof in Example 3.4.1 shows that the conclusion is valid for N = 1,2). The theorem then follows from Proposition 1, noting that both $\phi+\eta$ and $\phi-\eta$ and both $\boldsymbol{r}+\boldsymbol{\xi}$ and $\boldsymbol{r}-\boldsymbol{\xi}$ belong to $\mathcal{S}$ and $\mathcal{V}$, respectively, for every $\phi\in S$, $\eta\in H_0^1(\Omega)$, and $\boldsymbol{r},\boldsymbol{\xi}\in L^\gamma(\mathcal{B},\mathbb{R}^M)$. □

2.3. The effective minimization problem

In general, and for the purpose of finite element implementation, we will consider solving the maximization problem locally. It turns out that maximizing the incremental potential with respect to $\boldsymbol{r}$ is equivalent to maximizing the incremental potential density (Lemma 1). Thus, the problem that governs the electrophysiology update reads

$$\min_{\phi\in\mathcal{S}}F_n[\phi], \tag{34}$$

where

$$F_n[\phi]:=\int_{\mathcal{B}}\max_{\boldsymbol{r}\in\mathbb{R}^M}g_n(\phi(\boldsymbol{x}),\nabla\phi(\boldsymbol{x}),\boldsymbol{r})\,\mathrm{d}\boldsymbol{x}-\int_{\partial\mathcal{B}_q}\phi(\boldsymbol{x})\bar{q}(\boldsymbol{x})\,\mathrm{d}S, \tag{35}$$

which, in view of (11) and (15), we write as

$$F_n[\phi]:=\int_{\mathcal{B}}\left\{\frac{1}{2}\nabla\phi(\boldsymbol{x})\cdot\boldsymbol{D}\nabla\phi(\boldsymbol{x})+f_n(\phi(\boldsymbol{x}),\boldsymbol{x})\right\}\mathrm{d}\boldsymbol{x}-\int_{\partial\mathcal{B}_q}\phi(\boldsymbol{x})\bar{q}(\boldsymbol{x})\,\mathrm{d}S \tag{36}$$

with

$$f_n(\phi,\boldsymbol{x})=\max_{\boldsymbol{r}\in\mathbb{R}^M}\left\{\Delta t\cdot\psi\left(\frac{\phi-\phi_n(\boldsymbol{x})}{\Delta t},\frac{\boldsymbol{r}-\boldsymbol{r}_n(\boldsymbol{x})}{\Delta t}\right)+F(\phi,\boldsymbol{r})\right\},\quad\phi\in\mathbb{R},\quad\boldsymbol{x}\in\mathcal{B}. \tag{37}$$

Lemma 1. *If for every $\phi\in\mathcal{S}$ there exists $\boldsymbol{r}_\phi\in\mathcal{V}$ such that*

$$\Delta t\cdot\psi\left(\frac{\phi(\boldsymbol{x})-\phi_n(\boldsymbol{x})}{\Delta t},\frac{\boldsymbol{r}_\phi(\boldsymbol{x})-\boldsymbol{r}_n(\boldsymbol{x})}{\Delta t}\right)+F(\phi(\boldsymbol{x}),\boldsymbol{r}_\phi(\boldsymbol{x}))=f_n(\phi(\boldsymbol{x}),\boldsymbol{x})\quad\forall\ \boldsymbol{x}\in\mathcal{B} \tag{38}$$

(i.e. if for every $\boldsymbol{x}\in\mathcal{B}$ it is possible to choose an $\boldsymbol{r}_\phi(\boldsymbol{x})$, at which the maximum in (37) is attained, in such a way that $\boldsymbol{r}_\phi:\mathcal{B}\to\mathbb{R}^M$, as a function of $\boldsymbol{x}$, belongs to $\mathcal{V}$), then

$$F_n[\phi]=\max_{\boldsymbol{r}\in\mathcal{V}}G_n[\phi,\boldsymbol{r}]\quad\forall\ \phi\in\mathcal{S}.$$

Proof. Let $\phi\in\mathcal{S}$ and suppose that (38) is satisfied. Then, on the one hand,

$$\max_{\boldsymbol{r}\in\mathcal{V}}G_n[\phi,\boldsymbol{r}]\geqslant G_n[\phi,\boldsymbol{r}_\phi] \tag{39}$$

$$=\int_{\mathcal{B}}\frac{1}{2}\nabla\phi\cdot\boldsymbol{D}\nabla\phi+\Delta t\,\psi\left(\frac{\phi-\phi_n}{\Delta t},\frac{\boldsymbol{r}_\phi-\boldsymbol{r}_n}{\Delta t}\right)+F(\phi,\boldsymbol{r}_\phi)\,\mathrm{d}\boldsymbol{x}-\int_{\partial\mathcal{B}_q}\phi\bar{q}\,\mathrm{d}S \tag{40}$$

$$=\int_{\mathcal{B}}\frac{1}{2}\nabla\phi\cdot\boldsymbol{D}\nabla\phi+f_n(\phi,\boldsymbol{x})\,\mathrm{d}\boldsymbol{x}-\int_{\partial\mathcal{B}_q}\phi\bar{q}\,\mathrm{d}S=F_n[\phi]. \tag{41}$$

On the other hand, for every $\boldsymbol{r}\in\mathcal{V}$

$$G_n[\phi,\boldsymbol{r}] = \int_{\mathcal{B}} \frac{1}{2}\nabla\phi\cdot\boldsymbol{D}\nabla\phi + \Delta t\,\psi\left(\frac{\phi-\phi_n}{\Delta t},\frac{\boldsymbol{r}-\boldsymbol{r}_n}{\Delta t}\right) + F(\phi,\boldsymbol{r})\,\mathrm{d}\boldsymbol{x} - \int_{\partial\mathcal{B}_q}\phi\bar{q}\,\mathrm{d}S \tag{42}$$

$$\leqslant \int_{\mathcal{B}} \frac{1}{2}\nabla\phi\cdot\boldsymbol{D}\nabla\phi + f_n(\phi(\boldsymbol{x}),\boldsymbol{x})\,\mathrm{d}\boldsymbol{x} - \int_{\partial\mathcal{B}_q}\phi\bar{q}\,\mathrm{d}S = F_n[\phi]. \tag{43}$$

Consequently, $\max_{\boldsymbol{r}\in\mathcal{V}} G_n[\phi,\boldsymbol{r}] \leqslant F_n[\phi]$, completing the proof. □

Typically, gradient-descent methods are employed in the numerical solution of (34). In particular, a Newton–Raphson iteration guarantees convergence of the method if the objective function is strictly convex [4]. However, if the function $F(\phi,r)$ defining the electrochemical potential density is non-convex, the convexity of the effective incremental potential cannot be guaranteed for large values of the time step Δt, limiting therefore the robustness and efficiency in the minimization procedure. This important limitation in the numerical solution of the electrophysiology update is overcome in Proposition 2, where it is shown that as $\Delta t \to 0$ the incremental potential becomes strictly convex, implying that the minimization algorithm will converge to the unique solution for sufficiently small Δt.

Proposition 2. *A sufficient condition for F_n to be strictly convex is that*

$$\frac{1}{\Delta t} > \frac{\delta_\phi}{C_\phi} - \frac{\mu}{C_\phi C_{\mathcal{B}}}, \tag{44}$$

where δ_ϕ, μ and $C_{\mathcal{B}}$ are as in Theorem 1.

Proof. For every ϕ and $\tilde{\phi} \in \mathbb{R}$

$$(1-\lambda)f_n(\phi) + \lambda f_n(\tilde{\phi}) \tag{45}$$

$$\geqslant \max_{\boldsymbol{r}\in\mathbb{R}^M}\left\{(1-\lambda)\left(\Delta t\,\psi\left(\frac{\phi-\phi_n}{\Delta t},\frac{\boldsymbol{r}-\boldsymbol{r}_n}{\Delta t}\right) + F(\phi,\boldsymbol{r})\right) + \lambda\left(h\psi\left(\frac{\tilde{\phi}-\phi_n}{\Delta t},\frac{\boldsymbol{r}-\boldsymbol{r}_n}{\Delta t}\right) + F(\tilde{\phi},\boldsymbol{r})\right)\right\}, \tag{46}$$

while for every $\boldsymbol{r} \in \mathbb{R}^M$

$$(1-\lambda)\Delta t\,\psi\left(\frac{\phi-\phi_n}{\Delta t},\frac{\boldsymbol{r}-\boldsymbol{r}_n}{\Delta t}\right) + \lambda\Delta t\,\psi\left(\frac{\tilde{\phi}-\phi_n}{\Delta t},\frac{\boldsymbol{r}-\boldsymbol{r}_n}{\Delta t}\right) - \Delta t\,\psi\left(\frac{(1-\lambda)\phi+\lambda\tilde{\phi}-\phi_n}{\Delta t},\frac{\boldsymbol{r}-\boldsymbol{r}_n}{\Delta t}\right) \geqslant \frac{\lambda(1-\lambda)}{2}\frac{C_\phi}{\Delta t}(\phi-\tilde{\phi})^2$$

and

$$(1-\lambda)F(\phi,\boldsymbol{r}) + \lambda F(\tilde{\phi},\boldsymbol{r}) - F((1-\lambda)\phi+\lambda\tilde{\phi},\boldsymbol{r}) \geqslant \frac{\lambda(1-\lambda)}{2}\left(\inf_{\mathbb{R}\times\mathbb{R}^M}\frac{\partial^2 F}{\partial\phi^2}\right)(\phi-\tilde{\phi})^2.$$

Therefore,

$$(1-\lambda)\left(\Delta t\,\psi\left(\frac{\phi-\phi_n}{\Delta t},\frac{\boldsymbol{r}-\boldsymbol{r}_n}{\Delta t}\right) + F(\phi,\boldsymbol{r})\right) + \lambda\left(\Delta t\,\psi\left(\frac{\tilde{\phi}-\phi_n}{\Delta t},\frac{\boldsymbol{r}-\boldsymbol{r}_n}{\Delta t}\right) + F(\tilde{\phi},\boldsymbol{r})\right)$$
$$\geqslant \left(\Delta t\,\psi\left(\frac{(1-\lambda)\phi+\lambda\tilde{\phi}-\phi_n}{\Delta t},\frac{\boldsymbol{r}-\boldsymbol{r}_n}{\Delta t}\right) + F((1-\lambda)\phi+\lambda\tilde{\phi},\boldsymbol{r})\right) + \frac{\lambda(1-\lambda)}{2}\left(\frac{C_\phi}{\Delta t}-\delta_\phi\right)(\phi-\tilde{\phi})^2$$

for every $\boldsymbol{r} \in \mathbb{R}^M$ and

$$(1-\lambda)f_n(\phi) + \lambda f_n(\tilde{\phi}) \geqslant f_n((1-\lambda)\phi+\lambda\tilde{\phi}) + \frac{\lambda(1-\lambda)}{2}\left(\frac{C_\phi}{\Delta t}-\delta_\phi\right)(\phi-\tilde{\phi})^2.$$

All in all,

$$(1-\lambda)F_n[\phi] + \lambda F_n[\tilde{\phi}] - F[(1-\lambda)\phi+\lambda\tilde{\phi}] \geqslant \frac{\lambda(1-\lambda)}{2}\int_{\mathcal{B}}\left\{\nabla(\phi-\tilde{\phi})\cdot\boldsymbol{D}\nabla(\phi-\tilde{\phi}) + \left(\frac{C_\phi}{\Delta t}-\delta_\phi\right)(\phi-\tilde{\phi})^2\right\}\mathrm{d}\boldsymbol{x}$$
$$\geqslant \frac{\lambda(1-\lambda)}{2}\left(\frac{C_\phi}{\Delta t}+\frac{\mu}{C_{\mathcal{B}}}-\delta_\phi\right)\int_{\mathcal{B}}(\phi-\tilde{\phi})^2\,\mathrm{d}\boldsymbol{x}. \qquad \square$$

2.4. Spatial discretization: finite-element approximation

In the following, we shall be concerned with finding an approximate solution to problem (34). To this end, we pursue a finite-element formulation based on the Ritz method. For the sake of clarity, we omit the time-related sub-indices in the following. We perform the spatial approximation by considering a finite-dimensional approximating space $\mathcal{S}^h \subset \mathcal{S}$. The basis

$\{N_1, N_2, \ldots, N_m\} \in \mathcal{S}^h$ is systematically constructed upon a finite-element partition $\mathcal{B}^h$ of the domain $\mathcal{B}$, where the superindex h indicates the dependence on the mesh size. Thus, any element $\phi^h \in \mathcal{S}^h$ can be uniquely expanded as

$$\phi^h = \sum_{a=1}^{m} N_a u_a, \tag{47}$$

where $u_a \in \mathbb{R}, a = 1, \ldots, m$. We consider finite-element basis such that the Kronecker-delta property is satisfied, that is,

$$N_a(\boldsymbol{x}_b) = \begin{cases} 1 & a = b \\ 0 & a \neq b \end{cases}.$$

We then look for a solution to the approximate problem

$$\min_{\phi \in \mathcal{S}^h} F_n[\phi] = \min_{\boldsymbol{u} \in \mathbb{R}^m} F_n^h(\boldsymbol{u}), \tag{48}$$

where $\boldsymbol{u} = [u_1, \ldots, u_m]$ and

$$F_n^h(\boldsymbol{u}) = \int_{\mathcal{B}^h} \left\{ \sum_{a=1}^{m} \sum_{b=1}^{m} \frac{1}{2} \nabla N_a \cdot \boldsymbol{D} \nabla N_b u_a u_b + f_n \left(\sum_{a=1}^{m} N_a u_a \right) \right\} \mathrm{d}\boldsymbol{x} - \int_{\partial \mathcal{B}_q^h} \sum_{a=1}^{m} N_a \bar{q} u_a \, \mathrm{d}S, \tag{49}$$

where we have omitted the dependence on the position $\boldsymbol{x}$ of the terms in the integrand, for simplicity.

Proposition 3. *Under condition (44), the minimization problem (48) is a convex problem and has a unique solution $\boldsymbol{U}^* \in \mathbb{R}^m$. Moreover, if $\boldsymbol{u} \mapsto f_n(\sum_a^m N_a(\boldsymbol{x}) u_a, \boldsymbol{x}) \in C^1(\mathbb{R}^m)\ \forall\ \boldsymbol{x} \in \mathcal{B}$, then the optimal point $\boldsymbol{U}^*$ is characterized by the optimality condition*

$$DF_n^h(\boldsymbol{U}^*) = \boldsymbol{0}, \tag{50}$$

where

$$\left[DF_n^h(\boldsymbol{u}) \right]_a = \int_{\mathcal{B}^h} \left\{ \sum_{b=1}^{m} \nabla N_a \cdot \boldsymbol{D} \nabla N_b u_b + \frac{\partial}{\partial \phi} f_n \left(\sum_{a=1}^{m} N_a u_a \right) N_a \right\} \mathrm{d}\boldsymbol{x} - \int_{\partial \mathcal{B}_q^h} N_a \bar{q} \, \mathrm{d}S. \tag{51}$$

Proof. Let $\boldsymbol{u}, \tilde{\boldsymbol{u}} \in \mathbb{R}^m$, $\phi = \sum_{a=1}^m N_a u_a$, $\tilde{\phi} = \sum_{a=1}^m N_a \tilde{u}_a$ and $\lambda \in (0, 1)$. We note that

$$F_n^h((1-\lambda)\boldsymbol{u} + \lambda \tilde{\boldsymbol{u}}) = F_n[(1-\lambda)\phi + \lambda \tilde{\phi}] < (1-\lambda) F_n[\phi] + \lambda F_n[\tilde{\phi}] = (1-\lambda) F_n^h(\boldsymbol{u}) + \lambda F_n^h(\tilde{\boldsymbol{u}}) \tag{52}$$

and therefore F_n^h is a strictly convex function in $\mathbb{R}^m$. Standard results for unconstrained optimization of strictly convex objective functions (see, e.g., [4]) guarantee the existence and uniqueness of the optimal point $\boldsymbol{U}^* \in \mathbb{R}^m$. The smoothness condition on f_n implies the existence of the first tangent $DF_n^h : \mathbb{R}^m \to \mathbb{R}^m$ described in (51), and therefore the optimality condition (50) follows from standard results of convex optimization. □

Remark 3. Tipically, the minimization problem (48) is solved using gradient-descent methods where the first, and possibly the second tangent of (49) are required. Assuming $\boldsymbol{u} \mapsto f_n(\sum_a^m N_a(\boldsymbol{x}) u_a, \boldsymbol{x}) \in C^2(\mathbb{R}^m)\ \forall\ \boldsymbol{x} \in \mathcal{B}$, it follows that the components of the second tangent take the form

$$\left[D^2 F_n^h(\boldsymbol{u}) \right]_{ab} = \int_{\mathcal{B}^h} \left\{ \nabla N_a \cdot \boldsymbol{D} \nabla N_b + \frac{\partial^2}{\partial \phi^2} f_n \left(\sum_{a=1}^{m} N_a u_a \right) N_a N_b \right\} \mathrm{d}\boldsymbol{x},$$

which is always symmetric since it derives from a potential.

We shall not prove in this work the convergence of the finite-element approximation scheme as the mesh size $h \to 0$. However, we note that the convergence of finite-element approximations for variational formulations of non-linear problems of the type here presented, including convergence of numerical quadrature, has been recently addressed using $\Gamma-$convergence [10] in the context of quantum mechanics [18,43,28]. We remark that for the particular case of the Fitz-Hugh–Nagumo model, error estimates for the Galerkin finite-element approximation have been derived by Sanfelici [41].

Remark 4 (*Poincaré constant*). The Poincaré constant can be numerically approximated using a finite-element scheme, as we show next. Let $\mathcal{S} = \eta \in H^1(\mathcal{B})$ s.t. $\eta = 0$ on $\partial \mathcal{B}_\phi$ be the space of admissible solutions and $\mathcal{S}^h \subset \mathcal{S}$ be the corresponding finite-element approximating space. From (22) we can express the optimal Poincaré constant $C_{\mathcal{B}}$ in terms of the minimization problem

$$\frac{1}{C_{\mathcal{B}}} = \inf_{\eta \in \mathcal{S}} \frac{\int_{\mathcal{B}} |\nabla \eta(\boldsymbol{x})|^2 \, \mathrm{d}\boldsymbol{x}}{\int_{\mathcal{B}} \eta(\boldsymbol{x})^2 \, \mathrm{d}\boldsymbol{x}}, \tag{53}$$

where we recognize the objective function as the Rayleigh quotient. Therefore, the problem (53) is an eigenvalue problem, with $\lambda_{min} = \frac{1}{C_{\mathcal{B}}} \geqslant 0$ being the minimum eigenvalue. Using a finite-element approximation of the kind (47), we arrive at the classical finite-dimensional Rayleigh–Ritz problem

$$\lambda^h_{\min} = \min_{\boldsymbol{u}\in\mathbb{R}^m} \frac{\boldsymbol{u}^T\boldsymbol{K}\boldsymbol{u}}{\boldsymbol{u}^T\boldsymbol{M}\boldsymbol{u}} \tag{54}$$

where $\boldsymbol{K}, \boldsymbol{M} \in \mathbb{R}^{m\times m}$ are the stiffness and mass matrices, respectively, with components

$$K_{ab} = \int_{\mathcal{B}} \nabla N_a \cdot \nabla N_b \, \mathrm{d}\boldsymbol{x},$$
$$M_{ab} = \int_{\mathcal{B}} N_a N_b \, \mathrm{d}\boldsymbol{x}.$$

Due to the approximating property of the finite-element space $\mathcal{S}^h \subset \mathcal{S}$, it follows that $\lambda^h_{\min} \geqslant \lambda_{\min}$, and consequently $\frac{1}{\lambda^h_{\min}} \leqslant C_{\mathcal{B}}$. Classical finite-element error estimates show that $\lambda^h_{\min} \to \lambda_{\min}$ as $h \to 0$, and therefore $\frac{1}{\lambda^h_{\min}}$ can be used as an approximation to $C_{\mathcal{B}}$ for sufficiently fine meshes.

2.5. Application to the FitzHugh–Nagumo model

As an example of the application of the proposed variational formulation, we consider the FitzHugh–Nagumo equations of electrophysiology, in the form presented in [40,38]. The FitzHugh–Nagumo model and variants of it have been widely employed in modeling the cardiac activity in mammalian hearts. They consider one recovery variable ($M = 1$), and the source terms and the rate potential take the form

$$f^{\phi}(\phi, r) = c_1\phi\{\phi - \alpha\}\{1 - \phi\} - c_2 r, \tag{55}$$
$$f^{r}(\phi, r) = c_2\{\phi - d\, r\} \tag{56}$$

and

$$\Psi[\dot\phi, \dot r] := \int_{\mathcal{B}} \psi(\dot\phi, \dot r)\, \mathrm{d}\boldsymbol{x} = \int_{\mathcal{B}} \left\{\frac{1}{2}\dot\phi^2 - \frac{c_2}{2b}\dot r^2\right\} \mathrm{d}\boldsymbol{x}, \tag{57}$$

respectively, where $\alpha \in \mathbb{R}$ is a threshold parameter for electrical activation, $c_1 \in \mathbb{R}_+$ and $c_2 \in \mathbb{R}_+$ are excitation rate and excitation decay positive constants, respectively, and $b \in \mathbb{R}_+$ and $d \in \mathbb{R}_+$ are recovery rate and recovery decay positive constants, respectively. The generalized electrochemical potential takes the form

$$\begin{aligned}\mathcal{E}[\phi, r] &:= \int_{\mathcal{B}} E(\phi, \nabla\phi, r)\, \mathrm{d}\boldsymbol{x} + \int_{\mathcal{B}_q} \phi\bar q \, \mathrm{d}S \\ &= \int_{\mathcal{B}} \left\{\frac{1}{2}\nabla\phi\cdot\boldsymbol{D}\nabla\phi + c_1\left[\frac{1}{4}\phi^4 - \frac{(1+\alpha)}{3}\phi^3 + \frac{\alpha}{2}\phi^2\right] + c_2\left[\phi r - \frac{d}{2}r^2\right]\right\} \mathrm{d}\boldsymbol{x} + \int_{\mathcal{B}_q} \phi\bar q \, \mathrm{d}S,\end{aligned} \tag{58}$$

where $E : \mathbb{R}\times\mathbb{R}^N\times\mathbb{R} \to \mathbb{R}$ is the electrochemical potential density. Fig. 1(a) depicts the electrochemical potential density landscape for values typically employed in cardiac simulations. As anticipated, the electrochemical potential density may be non-convex, as shown in the plane cut $r = 0.5$ in Fig. 1(b).

Proposition 4. *Suppose that $N \leqslant 4$ and that either $c_1 C_{\mathcal{B}}(\alpha^2 - \alpha + 1) < 3\mu$ or*

$$\Delta t < \frac{1}{\frac{c_1}{3}(1 - \alpha + \alpha^2) - \frac{\mu}{C_{\mathcal{B}}}}, \tag{59}$$

where μ is the smallest eigenvalue of the conductivity tensor $\boldsymbol{D}$ and $C_{\mathcal{B}}$ is the Poincaré constant in (22). Then, the FitzHugh–Nagumo semi-discrete electrophysiology equations

$$\frac{\phi_{n+1} - \phi_n}{\Delta t} - \operatorname{div}(\boldsymbol{D}\nabla\phi_{n+1}) = f^{\phi}(\phi_{n+1}, r_{n+1}), \tag{60}$$
$$\frac{r_{n+1} - r_n}{\Delta t} = \frac{b}{c_2} f^{r}(\phi_{n+1}, r_{n+1}), \tag{61}$$

admit a unique weak solution (ϕ_{n+1}, r_{n+1}) determined by the relations

$$F_n[\phi_{n+1}] = \min_{\substack{\phi\in H^1(\mathcal{B}) \\ \phi=\bar\phi \text{ on } \partial\mathcal{B}_\phi}} F_n[\phi] \quad \text{and} \quad r_{n+1} = \frac{r_n + b\Delta t\phi_{n+1}}{1 + bd\,\Delta t}, \tag{62}$$

where $F_n[\phi]$, which is given by (36), is strictly convex.

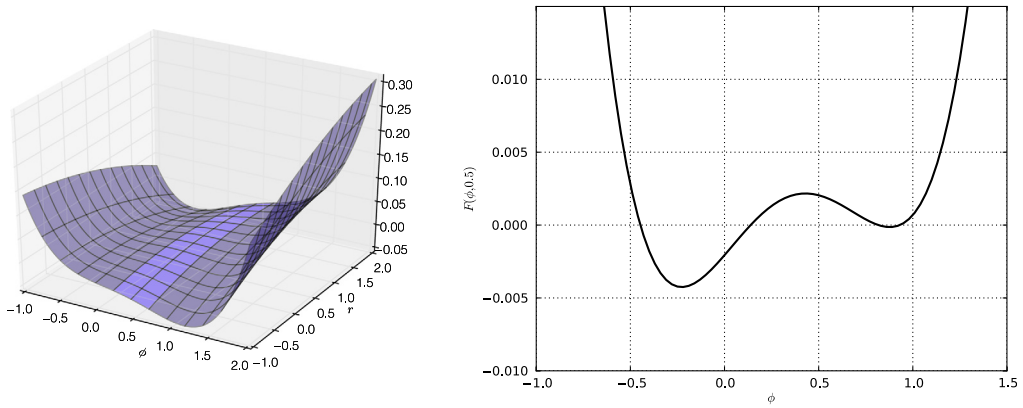

(a) Electrochemical energy landscape

(b) Energy landscape non-convex slice ($r = 0.5$)

Fig. 1. Energy landscape for the electrochemical potential density using $\alpha = 0.12, c_1 = 0.175, c_2 = 0.03, b = 0.011$ and $d = 0.55$.

Proof. The proposition follows from Theorem 1, Lemma 1 and Proposition 2, once we check that

$$F(\phi, r) = c_1\left(\frac{1}{4}\phi^4 - \frac{(1+\alpha)}{3}\phi^3 + \frac{\alpha}{2}\phi^2\right) + c_2\left(\phi r - \frac{d}{2}r^2\right) \tag{63}$$

satisfies the hypotheses (17)–(19) with $\gamma = 2$, that

$$\sup_{\mathbb{R}\times\mathbb{R}} \frac{\partial f^\phi}{\partial \phi}(\phi, r) = \frac{c_1}{3}(1 - \alpha + \alpha^2) > 0 \tag{64}$$

and that

$$\frac{(\phi - \phi_n)^2}{2\Delta t} - \frac{c_2(r - r_n)^2}{2b\Delta t} + F(\phi, r) = f_n(\phi, \boldsymbol{x}) \quad \Longleftrightarrow \quad r = \frac{r_n + b\Delta t\phi}{1 + bd\,\Delta t} \tag{65}$$

(the condition in (38) holds automatically since $r_n + b\Delta t\phi \in L^2$ whenever $r_n \in L^2$ and $\phi \in H^1$). In order to prove (17) it suffices to observe that

$$|F(\phi, r)| \leqslant \left(\frac{c_1}{4}|\phi|^4 + \frac{c_1(1+\alpha)}{3}(|\phi|^4 + 1) + \frac{c_1\alpha}{2}(|\phi|^4 + 1)\right) + c_2\left(\frac{\phi^2 + r^2}{2} - \frac{d}{2}r^2\right) \tag{66}$$

$$\leqslant \left(\frac{c_1}{4} + \frac{c_1(1+\alpha)}{3} + \frac{c_1\alpha}{4} + \frac{c_2}{2}\right)|\phi|^4 + \frac{c_2 + d}{2}r^2 + c_1\left(\frac{1+\alpha}{3} + \frac{\alpha}{4}\right). \tag{67}$$

Conditions (F18) and (F19) are proved analogously. The value of $\sup \frac{\partial f^\phi}{\partial \phi}$ is obtained from

$$\frac{\partial f^\phi}{\partial \phi} = -3c_1\left(\phi - \frac{1+\alpha}{3}\right)^2 + \frac{c_1}{3}(1 - \alpha + \alpha^2)$$

and (65) holds because the expression on the left is quadratic in r. □

From (59) we see that knowing μ and $C_{\mathcal{B}}$ improves the time-step upper bound, and indeed it can be numerically verified that the finite element method remains robust and stable for larger time steps as the ellipticity of the system (measured by μ) increases, as we show in the next section. Nevertheless, the dependence of the Poincaré constant $C_{\mathcal{B}}$ on $\mathcal{B}$ and $\partial\mathcal{B}_\phi$ is, in general, very hard to make explicit (see, e.g. [46]).

When dealing with a pure Dirichlet problem (i.e. when $\partial B_\phi = \partial\mathcal{B}$), $C_{\mathcal{B}}$ is the reciprocal of the first Dirichlet eigenvalue of the Laplacian and can be bounded above, for example, by the thickness of $\mathcal{B}$ (this can be seen by a careful inspection of the proof of the Gagliardo–Nirenberg inequality [13], the monotonicity of the Dirichlet eigenvalues with respect to the domain and a standard domain decomposition argument). At the opposite end, in the case of a pure Neumann problem (when $\partial B_\phi = \varnothing$), the constant $C_{\mathcal{B}}$ depends on the diameter of the domain and on the curvature of its boundary in a very subtle manner ($C_{\mathcal{B}}$ blows up as the domain becomes less and less connected, as when a rectangle is pinched in the middle, in a way that is difficult to quantify, see, e.g. [5, Theorem 1.1]). As already mentioned in Remark 4, for arbitrary geometries the constant $C_{\mathcal{B}}$ can be approximated by the minimum eigenvalue of the finite-element discretization of the Rayleigh–Ritz problem.

Remark 5. Due to the above considerations, a weaker upper bound for the time-step size, which, by virtue of Proposition 4, still guarantees the strict convexity of F_n and the well-posedness of the minimax problem for arbitrary domains is:

$$\Delta t < \frac{3}{c_1(1-\alpha+\alpha^2)}. \tag{68}$$

3. Numerical examples

To demonstrate the applicability of the proposed variational update in the time integration of electrophysiological systems, we start by considering the simulation of a single-cell, where a spatially-uniform response is assumed and spatial dependence is usually neglected. This is equivalent to setting the conductivity tensor to zero, and the effective minimization problem (34) reduces to the unconstrained minimization of the effective density $f_n(\phi)$. Typical parameter values for the FitzHugh–Nagumo model used in cardiac-tissue simulations are given in Table 1. For initial conditions, we have set $\phi|_{t=0} = 0.2,\ r|_{t=0} = 0$. These values ensure the activation of the cell, given that the initial potential is greater than the threshold potential α for a cell in resting condition ($r = 0$). Using a Newton–Raphson solver and setting the time-step size to $\Delta t = 10$ ms, we have determined the time evolution of the transmembrane potential and recovery variable for the time interval $[0, 800]$ ms, see Fig. 2. For all practical matters, in single-cell simulations $N \leqslant 3$, and we note that the smallest eigenvalue of the conductivity tensor is $\mu = 0$. Let

$$\Delta t^{\text{sc}}_{\text{convex}} := \frac{3}{c_1(1-\alpha+\alpha^2)} = 18.5 \text{ ms}. \tag{69}$$

Thus, from Proposition 4 we have that

$$\Delta t < \Delta t^{\text{sc}}_{\text{convex}} = 18.5 \text{ ms}$$

is the condition that guarantees strict convexity in the effective minimization problem. To see the applicability of the time-step upper bound $\Delta t^{\text{sc}}_{\text{convex}}$, we have performed time-history calculations for several values of $\Delta t > \Delta t^{\text{sc}}_{\text{convex}}$ and $\Delta t < \Delta t^{\text{sc}}_{\text{convex}}$. From these calculations, we have obtained the error in each iteration from the evaluation of the residual norm, which in this case corresponds to the absolute value of the first derivative of the effective energy density. Fig. 3 shows the error versus the number of iterations for those time steps in which the number of iterations required to achieve an error below 10^{-10} was the largest. We see that for $\Delta t < \Delta t^{\text{sc}}_{\text{convex}}$, the error tolerance is quickly achieved in at most 3 iterations and quadratic convergence is observed in all cases. In contrast, cases where $\Delta t > \Delta t^{\text{sc}}_{\text{convex}}$ show lower order of convergence for a considerable number of iterations before they achieve quadratic convergence (case $\Delta t = 25$ ms), or no convergence at all in other cases ($\Delta t = \{33.3, 50.0\}$ ms), for a maximum number of iterations set to 20.

We now consider the case of electrical propagation in a rectangular block with spatial domain $\mathcal{B} = [0, 100] \times [0, 100] \times [0, 20] \subset \mathbb{R}^3$, where the length units are in millimeters. We have assumed a surface source of fixed transmembrane voltage in the yz-plane at $x = 0$ with domain $[0, 20] \times [4.8, 5.2]$ where the transmembrane potential is set to $\phi = 1$. In the remaining boundary, a zero-flux condition has been imposed. We consider the general case of a transversely isotropic conductivity tensor of the form

$$\boldsymbol{D} = d_{\text{iso}}\boldsymbol{I} + d_{\text{ort}}\boldsymbol{n} \otimes \boldsymbol{n}$$

where $d_{\text{iso}} \in \mathbb{R}_+$ corresponds to the isotropic conductivity, $\boldsymbol{I}$ is the unit tensor and $d_{\text{ort}} \in \mathbb{R}_+$ corresponds to the increase of conductivity in the $\boldsymbol{n}$ direction, and we note that isotropic conductivity is recovered by setting $d_{\text{ort}} = 0$. All the remaining parameters have been set to the values indicated in Table 1. All simulations have been performed using a finite-element mesh with 1200 tetrahedral linear elements otherwise indicated, and a standard Newton–Raphson solver was employed for all the minimization problems involved. We have considered two cases: an isotropic block with $d_{\text{iso}} = 1$ mm^2/ms and a transversely isotropic block with $d_{\text{iso}} = 0.1$ mm^2/ms, $d_{\text{ort}} = 0.9$ mm^2/ms and $\boldsymbol{n} = [1, 0, 0]^T$. The time evolution of the transmembrane potential field for the transversely isotropic block is shown in Fig. 4, where the time step has been set to $\Delta t = 12$ ms. We observe that the method is able to capture the preferential direction $\boldsymbol{n}$ of electrical propagation dictated by the conductivity tensor, as expected.

To study the robustness of the Newton–Raphson solver, we have analyzed the convergence of the method for several values of the time-step interval. As noted in Remark 5, the sub-optimal upper bound $\Delta t^{\text{sc}}_{\text{convex}} = 18.5$ ms defined in (69) applies in this case. We have carried out numerical simulations considering time steps smaller and greater than $\Delta t^{\text{sc}}_{\text{convex}}$ and have

Table 1
Parameter values for a single-cell example.

Parameter	Value	Units	Description
α	0.08	–	Normalized threshold potential
c_1	0.175	1/ms	Excitation rate constant
c_2	0.03	1/ms	Excitation decay constant
b	0.011	1/ms	Recovery rate constant
d	0.55	–	Recovery decay constant

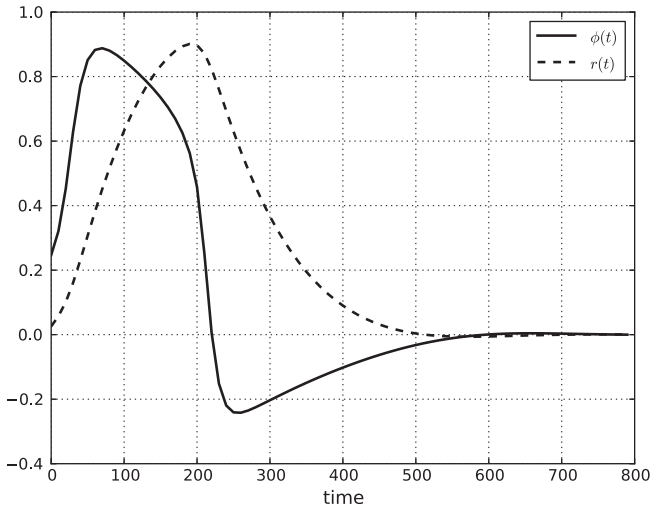

Fig. 2. Time evolution for a single-cell transmembrane potential and recovery variable.

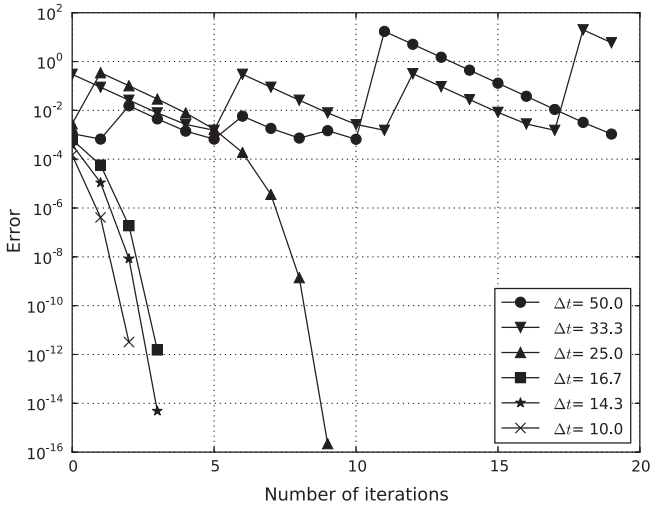

Fig. 3. Error plot for different time steps, $\Delta t_{\text{convex.}} = 18.5$ ms.

computed the residual error as a function of the number of iterations for the case with most iterations for the isotropic block and the transversely-isotropic block, which are shown in Fig. 5(a) and (b), respectively. We see that in both cases, simulations with $\Delta t < \Delta t^{sc}_{\text{convex}}$ quickly achieve the quadratically-convergent stage, as expected. To understand the influence of the conductivity tensor, we approximate the Poincaré constant by solving the minimum eigenvalue problem associated to the block geometry and boundary conditions, as explained in Remark 4, to obtain that $\frac{1}{C_B} \approx 9.683 \times 10^{-3}$. We further note that in the isotropic block, the minimum conductivity eigenvalue is $\mu = 1$ mm^2/ms, whereas in the transversely-isotropic block $\mu = 0.1$ mm^2/ms. Thus, evaluating the time-step bound (59) we obtain that $\Delta t < 22.55$ ms and $\Delta t < 18.54$ ms for the isotropic and transversely-isotropic blocks, respectively. Fig. (5(a)) shows that cases converging quadratically are in fact those where $\Delta t < 22.55$ ms, including the case $\Delta t = 20$ ms $> t^{sc}_{\text{convex}}$. In contrast, in Fig. (5(b)) the case $\Delta t = 20$ ms does not converge quadratically from the initial guess and takes many more iterations to converge, while cases with greater time-step size do not converge for a maximum number of iterations set equal to 20.

As a final example, and to demonstrate the applicability of the method in clinical applications, we consider a human biventricular domain determined from magnetic-resonance images of a healthy volunteer. The finite-element mesh is composed by 37,127 linear tetrahedral elements and 8,612 nodes, and is shown in Fig. 6. To obtain values of the transmembrane potential within the physiological range, the potential ϕ is rescaled as

$$\Phi = 110\phi - 80 \text{ [mV]}.$$

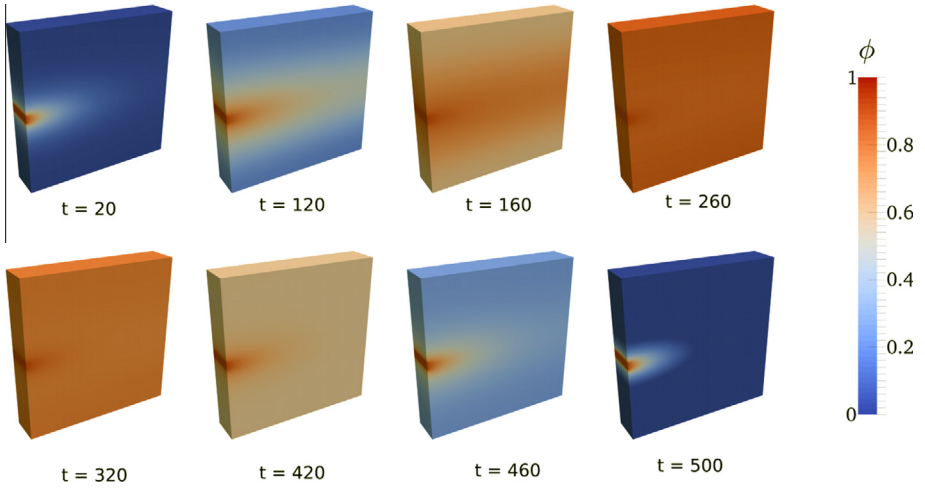

Fig. 4. Transmembrane potential field for a rectangular block with transversely-isotropic conductivity tensor.

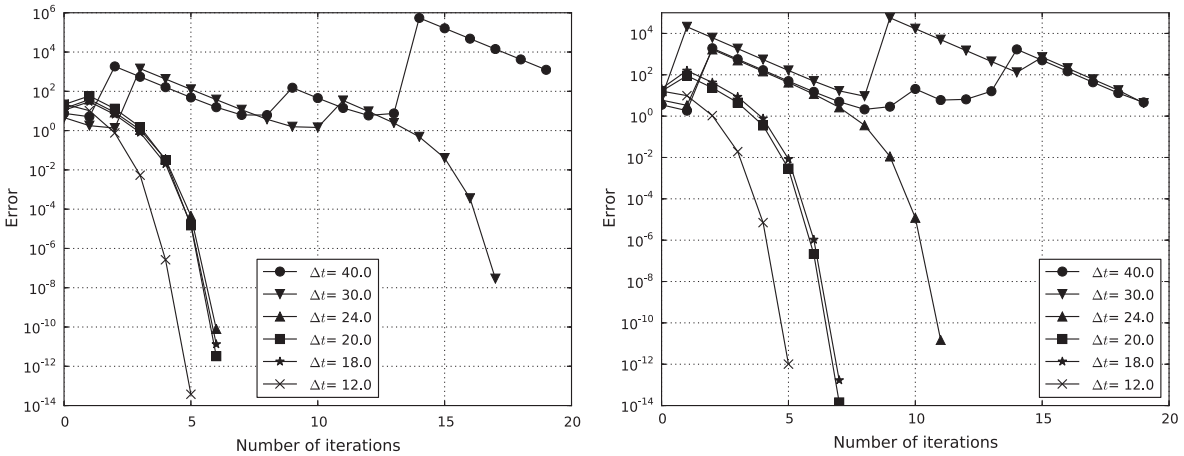

(a) Isotropic block (b) Transversely-isotropic block

Fig. 5. Residual error versus number of iterations for the rectangular block example.

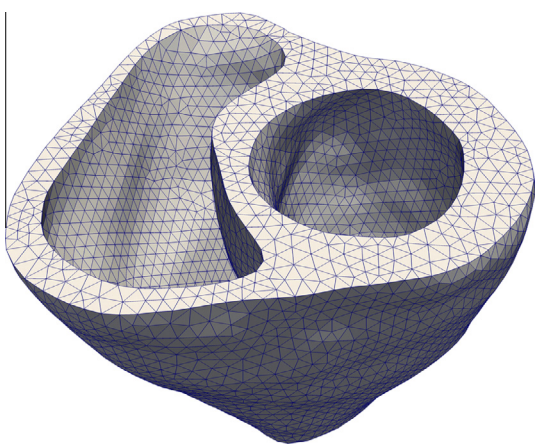

Fig. 6. Human biventricular finite-element mesh.

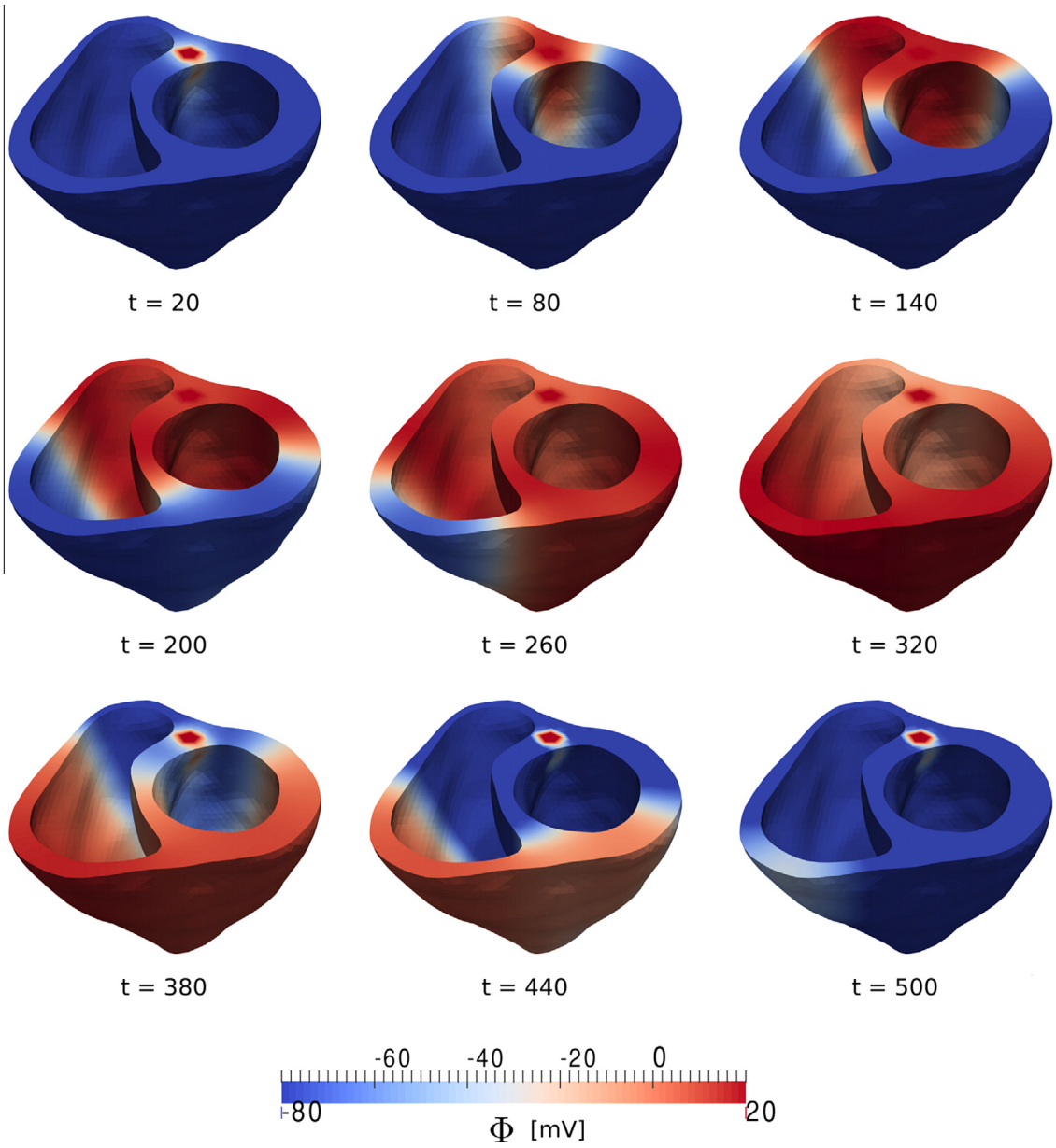

Fig. 7. Evolution of the transmembrane potential in a human biventricular model.

We have considered the model constants described in Table 1. The transversely-isotropic conductivity tensor constants were set to $d_{\text{iso}} = 1$ mm^2/ms and $d_{\text{ort}} = 14$ mm^2/ms with $\boldsymbol{n}$ being the apico-basal direction, to approximately reflect the highly-conducting nature of the Purkinjee fibers found in cardiac tissue. The boundary of the biventricular mesh has been prescribed with no-flux condition everywhere but in a small region where the atrio-ventricular node is located, where the rescaled transmembrane potential is set to $\Phi = 20$ mV for the whole duration of the simulation. Setting the time-step size to $\Delta t = 20$ ms, we have computed the transmembrane potential map for a number of points within the time interval $[0, 500]$ ms, which are shown in Fig. 7. We clearly observe how the electrical wave originated at the atrio-ventricular node propagates down through the septum wall, to reach the outer ventricular walls, eventually activating the whole biventricular domain at around $t = 320$ ms, to continue with the repolarization phase of cardiac activity and going back to the resting state at approximately $t = 500$ ms.

The convergence error of the Newton–Raphson iterations for several time-step values has been recorded for a number of simulations, see Fig. 8. For the particular biventricular geometry and boundary conditions, the minimum eigenvalue problem (54) yields $\frac{1}{C_g} \approx 1.21 \times 10^{-4}$, and we note that for the chosen conductivity tensor $\mu = 1$ mm^2/ms. Consequently, from (59) we

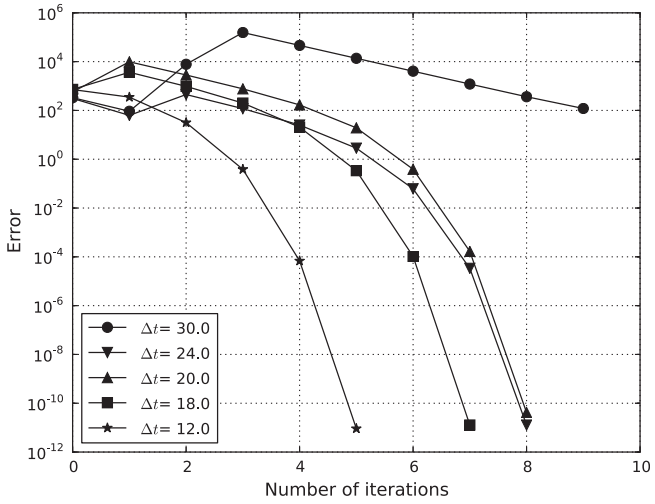

Fig. 8. Residual error versus number of iterations for the human biventricular example.

obtain that $\Delta t < 18.54$ ms, which represents only a slight improvement from $\Delta t^{\text{sc}}_{\text{convex}} = 18.5$ ms. We do, however, observe reasonable convergence for cases up to $\Delta t = 24$ ms, whereas the case $\Delta t = 30$ ms does not converge for a maximum number of iterations of 20.

4. Discussion

In this work, we have reformulated the general problem of electrical conduction in cardiac tissue as a gradient flow, and its temporal discretization as an equivalent variational principle. As anticipated, there are both, theoretical and numerical consequences that stem from this reformulation. From the theoretical point of view, the proposed variational principle lends itself to rigorous mathematical analysis addressing the existence of weak solutions of the time-discretized governing equations. It is worth remarking that the gradient flow and variational principle introduced in this work require the postulation of electrochemical and rate potentials, which are not necessarily available, or may be difficult to find for all electrophysiology models reported to date. An interesting avenue of research is the determination of what models can be expressed in terms of generalized potentials, and therefore conform to the proposed variational framework, for which the results reported in this work can be applied. Also, new models can be derived from the present gradient-flow formulation and the direct postulation of electrochemical potentials, which can be physically motivated based on smaller-scales mechanisms, potentially allowing for multiscale modeling.

From a numerical analysis standpoint, the existence and uniqueness of the solution of the saddle-point variational problem pose conditions on the time-step size that only depend on the model potentials and parameters. When analyzing the effective minimization problem, the conditions on the time-step size also guarantee the strict convexity of the incremental problem. In particular, we have shown that a finite-element spatial discretization yields to a convex problem with strictly convex objective function, for which convergence of gradient-descent methods is assured. Therefore, the time-step bounds presented in this work represent an important step toward improving the robustness of cardiac electrophysiology simulations. It is important to remark that the time-step bound given by Eq. (68), which is used extensively in the analysis of the results in Section 3 can be improved by the bound (59) if the optimal Poincaré constant and the conductivity-tensor smallest eigenvalue can be estimated via the finite-dimensional Rayleigh–Ritz problem. It follows from the definition of the conductivity tensor (3) that the smallest eigenvalue of the conductivity tensor is $\mu = d_{\text{iso}}$. Therefore, in the example of rectangular blocks, Proposition 4 yields a greater upper bound in the case of the isotropic block, since its conductivity-tensor smallest eigenvalue $\mu_{\text{iso}} = 1.0$ is greater than the smallest eigenvalue of the transversely-isotropic block $\mu_{\text{tra}} = 0.1$, while the Poincaré constant is the same in both cases. This observation has important implications in the application of numerical methods in computational cardiology, where transversely-isotropic conductivity tensors that account for the fiber-reinforced microstructure seen in cardiac-muscle tissue are the gold standard. We therefore conclude that the conductivity of the cardiac tissue matrix, and not that of the fibers, controls the time-step bound that guarantees the convergence of the non-linear solve. This observation is particularly relevant in the simulation of pathological cases in diseased hearts like bundle branch block or myocardial infarction, where the electrical conduction is severely decreased in localized regions of the Bundle of His or in the myocardium, respectively.

In all the numerical simulations carried out in this work we have employed a Newton–Raphson scheme to solve the resulting nonlinear discrete weak form given by (50). At each iteration, a tangent matrix and residual vector are computed, and the linear system of equations corresponding to the linearization of (50) must be solved in order to update the solution.

We remark here that any electrophysiological model that can be recast in the variational framework proposed here will always result in symmetric tangent matrices, which will in addition be positive-definite as long as the time-step bound (44) is met, as indicated in Remark 3. We note that, in general, this is not the case for most finite-element formulations of cardiac electrophysiological models, where non-symmetric tangent matrices usually arise. A linear system of equations with a positive-definite symmetric matrix has several computational and theoretical advantages over non-symmetric systems, like being amenable to efficient iterative methods of numerical linear algebra which result in computing times that can be several times smaller than those needed for non-symmetric linear systems. This consideration become very relevant when dealing with large-scale problems that are solved using parallel-computing platforms, highlighting the superior efficiency guaranteed by the proposed scheme over traditional finite-element formulations of the cardiac electrophysiology problem.

We close by noting that many of the techniques from computational solid mechanics and plasticity based on variational principles can find applications on the proposed variational principle for electrophysiology. For example, re-meshing techniques [39] and arbitrary Lagrangian–Eulerian methods [31] based on variational principles can be extended to the framework proposed in this work.

Acknowledgments

This work has been motivated by stimulating discussions with Ellen Kuhl, Stanford University and Michael Ortiz, Caltech. We would like to thank the Biomedical Imaging Center at PUC for providing the heart medical images and Francisco Sahli for generating the heart mesh. The support of the Chilean Fondo Nacional de Ciencia y Tecnología (FONDECYT) through Grants #11121224 and #11110011, and the PUC-VRI Inicio Grant #54/2011 are greatly appreciated.

References

[1] R. Aliev, A.V. Panfilov, A simple two-variable model of cardiac excitation, Chaos Solitons Fractals 7 (3) (1996) 293–301.
[2] L. Ambrosio, N. Gigli, G. Savaré, Gradient Flows in Metric Spaces and in the Space of Probability Measures, second ed., Birkhäuser, Verlag AG, Basel, Boston, Berlin, 2008.
[3] B.Y.G.W. Beeler, H. Reutert, Reconstruction of the action potential of ventricular myocardial fibres, J. Physiol. 268 (1977) 177–210.
[4] S. Boyd, L. Vandenberghe, Convex Optimization, vol. 25, Cambridge University Press, 2004.
[5] R. Chen, Neumann eigenvalue estimate on a compact Riemannian manifold, Proc. Am. Math. Soc. 108 (4) (1990) 961–970.
[6] P. Colli Franzone, G. Savaré, Degenerate evolution systems modeling the cardiac electric field at micro and macroscopic level, Evolution Equations, Semigroups and Functional Analysis, 2002, pp. 1–26.
[7] R. Courant, Variational methods for the solution of problems for equilibrium and vibrations, Bull. Am. Math. Soc. 49 (1) (1943) 1–23.
[8] M. Courtemanche, W. Skaggs, A. Winfree, Stable three-dimensional action potential circulation in the FitzHugh–Nagumo model, Physica D 41 (1990) 173–182.
[9] B. Dacorogna, Introduction to the Calculus of Variations, Imperial College Press, London, 2009.
[10] E. De Giorgi, T. Franzoni, Sur un tipo di convergenza variazionale, Atti Acad. Naz. Linccei Rend. Cl. Sci. Fis. Mat. Natur. 8 (1975).
[11] I. Ekeland, R. Témam, Convex Analysis and Variational Problems, SIAM, Philadelphia, 1999.
[12] T. El Sayed, A. Mota, F. Fraternali, M. Ortiz, A variational constitutive model for soft biological tissues, J. Biomech. 41 (7) (2008) 1458–1466.
[13] L.C. Evans, Partial Differential Equations, American Mathematical Society, 1998.
[14] F.H. Fenton, E.M. Cherry, Models of cardiac cell, Scholarpedia 3 (8) (2008) 1868.
[15] F.H. Fenton, A. Karma, Vortex dynamics in three-dimensional continuous myocardium with fiber rotation: filament instability and fibrillation, Chaos 8 (1) (1998) 20–47.
[16] R. FitzHugh, Impulses and physiological states in theoretical models of nerve membrane, Biophys. J. 1 (6) (1961) 445–466.
[17] G. Friesecke, G. Dolzmann, Implicit time discretization and global existence for a quasi-linear evolution equation with nonconvex energy, SIAM J. Math. Anal. 28 (2) (1997) 363.
[18] V. Gavini, J. Knap, K. Bhattacharya, M. Ortiz, Non-periodic finite-element formulation of orbital-free density functional theory, J. Mech. Phys. Solids 55 (4) (2007) 669–696.
[19] S. Göktepe, E. Kuhl, Computational modeling of cardiac electrophysiology: a novel finite element approach, Int. J. Numer. Methods Eng. 79 (2) (2009) 156–178.
[20] J. Guccione, G. Kassab, M. Ratcliffe (Eds.), Computational Cardiovascular Mechanics: Modeling and Applications in Heart Failure, Springer, New York, Dordrecht, Heidelberg, London, 2010.
[21] D.M. Harrild, C.S. Henriquez, A finite volume model of cardiac propagation, Ann. Biomed. Eng. 25 (2) (1997) 315–334.
[22] A. Hodgkin, A. Huxley, A quantitative description of membrane current and its application to conduction and excitation in nerve, J. Physiol. 117 (1952) 500–544.
[23] D.E. Hurtado, E. Kuhl, Computational modelling of electrocardiograms: repolarisation and T-wave polarity in the human heart, Comput. Methods Biomech. Biomed. Eng., in press, http://dx.doi.org/10.1080/10255842.2012.729582.
[24] D.E. Hurtado, M. Ortiz, Surface effects and the size-dependent hardening and strengthening of nickel micropillars, J. Mech. Phys. Solids 60 (8) (2012) 1432–1446.
[25] D.E. Hurtado, M. Ortiz, Finite element analysis of geometrically necessary dislocations in crystal plasticity, Int. J. Numer. Methods Eng. 93 (1) (2013) 66–79.
[26] P.R. Johnston, A finite volume method solution for the bidomain equations and their application to modelling cardiac ischaemia, Comput. Methods Biomech. Biomed. Eng. 13 (2) (2010) 157–170.
[27] J. Keener, J. Sneyd, Mathematical physiology: cellular physiology, Interdisciplinary Applied Mathematics, vol. 1, Springer Verlag, New York, NY, 1998.
[28] B. Langwallner, C. Ortner, E. Süli, Existence and convergence results for the Galerkin approximation of an electronic density functional, Math. Models Methods Appl. Sci. 20 (12) (2010) 2237–2265.
[29] G.T. Lines, M.L. Buist, P. Grottum, A.J. Pullan, J. Sundnes, A. Tveito, Mathematical models and numerical methods for the forward problem in cardiac electrophysiology, Comput. Visual. Sci. 5 (2003) 215–239.
[30] C.H. Luo, Y. Rudy, A dynamic model of the cardiac ventricular action potential. I. Simulations of ionic currents and concentration changes, Circ. Res. 74 (6) (1994) 1071–1096.
[31] J. Mosler, M. Ortiz, On the numerical implementation of variational arbitrary Lagrangian–Eulerian (VALE) formulations, Int. J. Numer. Methods Eng. 67 (9) (2006) 1272–1289.
[32] J. Nagumo, S. Arimoto, S. Yoshizawa, An active pulse transmission line simulating nerve axon, Proc. IRE 50 (10) (1962) 2061–2070.

[33] S.A. Niederer, E. Kerfoot, A.P. Benson, M.O. Bernabeu, O. Bernus, C. Bradley, E.M. Cherry, R. Clayton, F.H. Fenton, A. Garny, E. Heidenreich, S. Land, M. Maleckar, P. Pathmanathan, G. Plank, J.F. Rodríguez, I. Roy, F.B. Sachse, G. Seemann, O. Skavhaug, N.P. Smith, Verification of cardiac tissue electrophysiology simulators using an N-version benchmark, Philos. Trans. Ser. A Math. Phys. Eng. sci. 369 (2011) 4331–4351.
[34] D. Noble, A modification of the Hodgkin–Huxley equations applicable to Purkinje fibre action and pacemaker potentials, J. Physiol. 160 (1962) 317–352.
[35] M. Ortiz, L. Stainier, The variational formulation of viscoplastic constitutive updates, Comput. Methods Appl. Mech. Eng. 171 (1999) 419–444.
[36] A.V. Panfilov, J. Keener, Re-entry in an anatomical model of the heart, Chaos Solitons Fractals 5 (3–4) (1995) 681–689.
[37] M. Pennacchio, G. Savaré, P. Colli Franzone, Multiscale modeling for the bioelectric activity of the heart, SIAM J. Math. Anal. 37 (4) (2005) 1333.
[38] A.J. Pullan, M.L. Buist, L.K. Cheng, Mathematically Modelling the Electrical Activity of the Heart: From Cell to Body Surface and Back Again, World Scientific Publishing Co., Singapore, 2005.
[39] R. Radovitzky, M. Ortiz, Error estimation and adaptive meshing in strongly nonlinear dynamic problems, Comput. Methods Appl. Mech. Eng. 172 (1–4) (1999) 203–240.
[40] J.M. Rogers, A.D. McCulloch, A collocation-Galerkin finite element model of cardiac action potential propagation, IEEE Trans. Biomed. Eng. 41 (8) (1994) 743–757.
[41] S. Sanfelici, Convergence of the Galerkin approximation of a degenerate evolution problem in electrocardiology, Numer. Methods Partial Differ. Equ. 18 (2) (2002) 218–240.
[42] G.H. Sharp, R.W. Joyner, Simulated propagation of cardiac action potentials, Biophys. J. 31 (3) (1980) 403–423.
[43] P. Suryanarayana, V. Gavini, T. Blesgen, K. Bhattacharya, M. Ortiz, Non-periodic finite-element formulation of Kohn–Sham density functional theory, J. Mech. Phys. Solids 58 (2) (2010) 256–280.
[44] K.H.W.J. ten Tusscher, D. Noble, P.J. Noble, A.V. Panfilov, A model for human ventricular tissue, Am. J. Phys. Heart Circ. Physiol. 286 (4) (2004) H1573–H1589.
[45] N. Trayanova, Whole-heart modeling: applications to cardiac electrophysiology and electromechanics, Circ. Res. 108 (1) (2011) 113–128.
[46] A. Veeser, R. Verfurth, Poincaré constants for finite element stars, IMA J. Numer. Anal. 32 (1) (2011) 30–47.
[47] M. Veneroni, Reaction–diffusion systems for the macroscopic bidomain model of the cardiac electric field, Nonlinear Anal. Real World Appl. 10 (2) (2009) 849–868.
[48] E.J. Vigmond, F. Aguel, N. Trayanova, Computational techniques for solving the bidomain equations in three dimensions, IEEE Trans. Biomed. Eng. 49 (11) (2002) 1260–1269.
[49] K. Weinberg, M. Ortiz, Shock wave induced damage in kidney tissue, Comput. Mater. Sci. 32 (3–4) (2005) 588–593.
[50] J. Wong, S. Göktepe, E. Kuhl, Computational modeling of electrochemical coupling: a novel finite element approach towards ionic models for cardiac electrophysiology, Comput. Methods Appl. Mech. Eng. 200 (45–46) (2011) 3139–3158.